

## Measurements of recoil and projectile momentum distributions for 19-MeV $F^{9+}$ + Ne collisions

V. Frohne,<sup>1,\*</sup> S. Cheng,<sup>1,†</sup> R. M. Ali,<sup>1,‡</sup> M. L. A. Raphaelian,<sup>1,§</sup> C. L. Cocke,<sup>1</sup> and R. Olson<sup>2</sup>

<sup>1</sup>*J.R. Macdonald Laboratory, Physics Department, Kansas State University, Manhattan, Kansas 66506*

<sup>2</sup>*Department of Physics, University of Missouri at Rolla, Rolla, Missouri 65401*

(Received 5 October 1995)

The collision system of 19-MeV  $F^{9+}$  on Ne has been studied using recoil and projectile momentum spectroscopy. For each event, identified by final recoil and projectile charge state, the three-dimensional momentum vector of the recoil ion and the transverse momentum vector of the projectile ion were measured. The transverse momenta of the recoil and projectile ions were found to be equal in magnitude and opposite in direction, indicating that the transverse momentum exchange is dominated by interactions between the two ion cores. The transverse momentum distributions are well described by nCTMC calculations. The longitudinal momentum distributions of the recoil ions show that a large fraction of the momentum transferred to the projectile is carried off by continuum electrons. The recoil ions are scattered slightly backward, in partial agreement with predictions of nCTMC calculations.

PACS number(s): 34.50.Fa

### I. INTRODUCTION

The passage of fast charged particles through matter occurs in a wide range of situations such as ion implantation [1], radiation therapy [2], and heavy-ion pumped fusion [3]. For such applications, it is common to characterize the ion-matter interactions in terms of ranges, stopping powers, and angular scattering distributions. Such parameters describe the mean behavior of the collisions averaged over many collisions. In recent years considerable emphasis has been brought to bear on understanding the individual binary ion-atom encounters that ultimately determine the above average quantities. In this paper we examine the exchange of energy and momentum in the collision of 1-MeV/amu  $F^{9+}$  on Ne. Such a collision is typically a violent one, removing many electrons from the target, some of which may be captured by the originally bare projectile. The final states are sufficiently complex as to defy a complete experimental determination, and comprehensive electron spectroscopy on the outgoing electrons is nearly impossible. In this paper, we use measurements of the projectile and recoil momenta, and the charge states of these products, to experimentally isolate the final states and to deduce information on both transverse and longitudinal momentum transfer to the heavy-ion cores. Such an approach provides some of the same information that one could deduce from a complete electron momentum spectroscopy, but without the detection of the many individual continuum electrons. Instead, such heavy particle momentum spectroscopy provides, for each event, the equivalent of the average transverse continuum electron momentum and less complete information on the longitudinal momentum of the electrons.

Numerous measurements of the momenta or energies of the recoil ions produced in similar violent ion-atom encounters at MeV energies have been carried out in recent years [4–10]. Ullrich *et al.* measured the transverse energies of the recoil ions for fast  $U^{32+}$  on Ne and Ar [7] and found recoil energies ranging from thermal to several eV, depending on the recoil charge state. The results were found to be in good agreement with nCTMC calculations, one of only two theoretical approaches that has had significant success in dealing with such complex collisions. Levin *et al.* [5,6] used a time-of-flight technique to determine mean recoil energies for Cl and F projectiles on rare-gas targets for selected pairs of final recoil and projectile charges and were able to deduce characteristic impact parameters for the collisions and to demonstrate the importance of screening in the effective projectile-recoil potential. Additional total measurements were made by Grandin *et al.* [11]. The use of cooled targets by Ullrich *et al.* significantly improved the resolution possible in recoil ion momentum spectroscopy [8,10,12–14] and has been used to study both He and heavier targets. Further technical advancement by that group to the use of supersonically cooled He targets has now allowed very high-resolution complete recoil momentum spectroscopy to be carried out [9,15] and numerous studies of electron capture and ionization have been carried out (for a review, see Ullrich *et al.* [9]). Of particular relevance to the present work is the recent study of the transverse recoil energies for 10-MeV  $F^{8+}$  on Ne carried out by Lencinas *et al.* [16]. These authors found that the transverse momentum exchange was nearly entirely between projectile and recoil cores, with the continuum electrons carrying off at most a small net transverse momentum. They also found significant discrepancies between experiment and two theoretical predictions, namely, the nCTMC calculation [17] and calculations of Horbath based on a solution of the Vlasov equation [18].

While the transverse momentum exchange between heavy cores is closely tied to the impact parameter of the collision, the longitudinal momentum transfer is more closely related to the energy transfer or, in some cases, the operative “mechanism” in the collision. If no electrons are ejected into

\*Physics Department, Western Illinois University, Macomb, IL 61455.

†Physics Department, University of Toledo, Toledo, OH 43606.

‡Physics Department, University of Nevada at Reno, Reno, NV 89557.

§3340 Winter Park Drive No. 256, Sacramento, CA 95834.

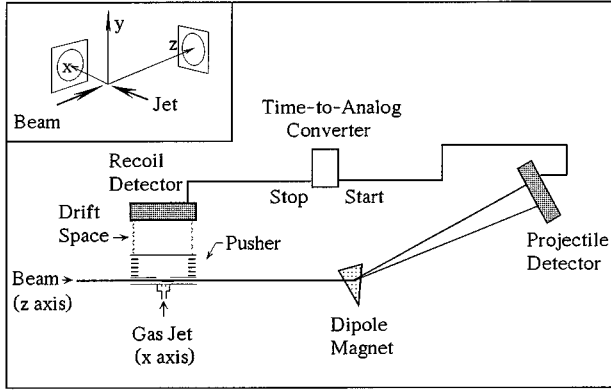


FIG. 1. Schematic of apparatus. Insert shows coordinate system used for analysis.

the continuum, as is the case for pure electron capture, there is a one-to-one relationship between longitudinal momentum transfer  $\Delta p_z$  and the release of electronic energy  $Q$  in the reaction. Several papers have reported the use of experimental determinations of longitudinal recoil momentum transfers to measure  $Q$  values for electron capture [8,15,19–22]. In addition, measurements of  $\Delta p_z$  can be used to distinguish collisions in which the recoil system acts as a unit from those in which the recoil ion is merely a spectator [23,24].

The complimentary measurement of the projectile longitudinal momentum change, or energy loss, is quite difficult, since it involves the daunting measurement of energy changes of a few hundred eV out of a projectile energy of several MeV. The experiments of Schuch *et al.* [25] and Schoene *et al.* [26] appear to be the only ones reported for high-velocity collisions of interest here. These authors were able to measure projectile energy losses up to several keV for MeV Cl and F ions colliding with rare-gas targets and to deduce that energy losses in the vicinity of 100–300 eV per continuum electron were typical in such collisions. Angular scattering distributions were also measured and good agreement with nCTMC calculations were found in those cases tested. These projectile energy-loss measurements are of direct relevance to the interpretation of the present results, since in principle both projectile and recoil momenta must be measured in order to deduce unambiguously the missing continuum electron momentum.

## II. EXPERIMENTAL METHOD

In this experiment we have measured, event by event, all three components of the recoil ion momentum, the two transverse components of the projectile momentum and the final charge states of both ions in 19-MeV  $F^{9+} + Ne$  collisions. For the purpose of discussion, the coordinate system for the experiment is defined in Fig. 1. The “longitudinal” direction is taken parallel to the beam, or  $z$ , direction and the transverse direction is perpendicular to the beam, in the  $x$ - $y$  plane. The schematic diagram of the apparatus is also shown in Fig. 1. The projectile ions were supplied by the KSU EN tandem Van de Graaff accelerator.  $F^{4+}$  ions were accelerated to 19 MeV (1 MeV/u) and then post stripped with a thin carbon foil to obtain 1-MeV/u  $F^{9+}$  ions. This beam was tightly collimated with four-jaw slits in order to produce a small cross-

section (typically  $0.2 \times 0.2$  mm<sup>2</sup>), parallel beam. The  $F^{9+}$  beam was magnetically charge-state analyzed immediately before the target region in order to ensure high charge-state purity. The gas jet target was an integral part of an assembly called the “pusher.” The recoil ions created in the pusher were extracted by a uniform electric field so that all recoil ions, regardless of initial direction, struck a two-dimensional position-sensitive detector. The projectile ions passed through the pusher, were charge-state analyzed, and were measured in coincidence with the recoil ions by another two-dimensional position-sensitive detector located 520 cm downstream. The detector used for the recoil ions was a 40-mm-diam. microchannel plate detector with a resistive anode. The projectile ion detector was either a 25-mm-diam. or a 40-mm-diam. microchannel plate detector using a backgammon (wedge and strip) anode. The combination of the pusher electric field, the projectile, and recoil detector position information, and the recoil ion time of flight provided the necessary information for the momentum reconstruction.

The projectile transverse momentum transfer was calculated from the position ( $XY$ ) at which the projectile hit on the downstream detector, using

$$P_x = Mv(X - X_{0p})/L,$$

$$P_y = Mv(Y - Y_{0p})/L, \quad (1)$$

where  $M$  is the projectile ion mass,  $v$  the incoming beam velocity, and  $X$  and  $Y$  the coordinates at which the ion hit the detector. The distance between the target and the projectile detector is  $L$  and  $X_{0p}$ ,  $Y_{0p}$  correspond to the position of an unscattered projectile on the detector. The recoil ion momentum vector for each event was calculated from the known position ( $y, z$ ) of the ion on the recoil detector, the time of flight (TOF), and a knowledge of the electric field in the pusher. The three components of the recoil ion momenta are given by

$$p_x = ma(t - t_0), \quad (2)$$

$$p_y = m(y - y_{0r})/t_0, \quad (3)$$

$$p_z = m(z - z_{0r})/t_0, \quad (4)$$

where  $t$  is the measured TOF of the recoil ion,  $t_0$  is the TOF of a recoil ion which had no initial velocity towards or away from the detector, e.g., a recoil ion that was scattered vertically in the collision,  $a$  is the ion acceleration in the pusher region, and  $m$  is the recoil ion mass. The acceleration was derived from the electric field  $E$  at the site of the collision in the pusher and is given by  $a = qeE/m$ , where  $e$  is the magnitude of the electronic charge. The centers  $y_{0r}$  and  $z_{0r}$  were taken to be the location at which  $Ne^{1+}$  ions in coincidence with  $F^{9+}$  projectiles struck the detector. The parameter  $t_0$  was taken to be the center of the time peak for each recoil charge state.

The main contributors to the finite momentum resolution for the recoil ions were the gas jet source size and thermal motion, and the detector time and position resolutions. The expected resolution function was calculated from the geometry and thermal properties of the collimated jet. The major contributor to the resolution function in the  $y$  direction was

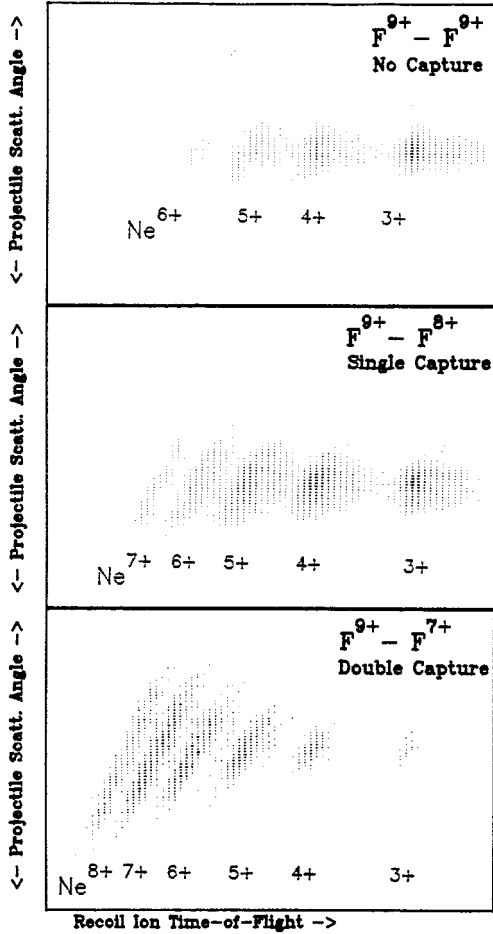


FIG. 2. Plots of recoil time of flight vs projectile position for three different final projectile charge states.

the thermal motion of that part of the gas jet traversed by a projectile beam of finite size. In the  $z$  direction, the thermal motion of the jet, and not the beam size, dominated the resolution function. The thermal contribution to  $p_z$  was larger because the beam creates recoil ions along a longer length in the  $z$  direction than in the  $y$  direction. In the  $x$ , or time, direction, the momentum distribution of the target is that of a collimated Maxwell-Boltzmann distribution flowing into a solid angle given by the intersection of the beam and the jet. A detailed model of the expected resolution from all sources gave calculated resolution functions characterized by widths  $\Delta p_x$ ,  $\Delta p_y$ , and  $\Delta p_z$  of 6.0, 5.5, and 10.5 a.u., full width at half maximum (FWHM). (We note the resolution function in the  $x$  direction is not centered at zero; only the FWHM is given here.) This result was checked experimentally using  $\text{Ne}^{1+}$  recoils in the  $\text{F}^{9+} \rightarrow \text{F}^{9+}$  channel, for which nCTMC calculations predict such small momentum transfers that the experimental results should be dominated by the resolution functions. Folding of a three-dimensional Gaussian experimental resolution function into the nCTMC results for this channel gave a best overall fit to the experimental results for this channel with  $\Delta p_x$ ,  $\Delta p_y$ , and  $\Delta p_z$  of 7.2, 7.2, and 12 a.u. (FWHM), respectively, close to the expected model results. The experimental Gaussian resolution functions were used in all further analysis of the data, as discussed below.

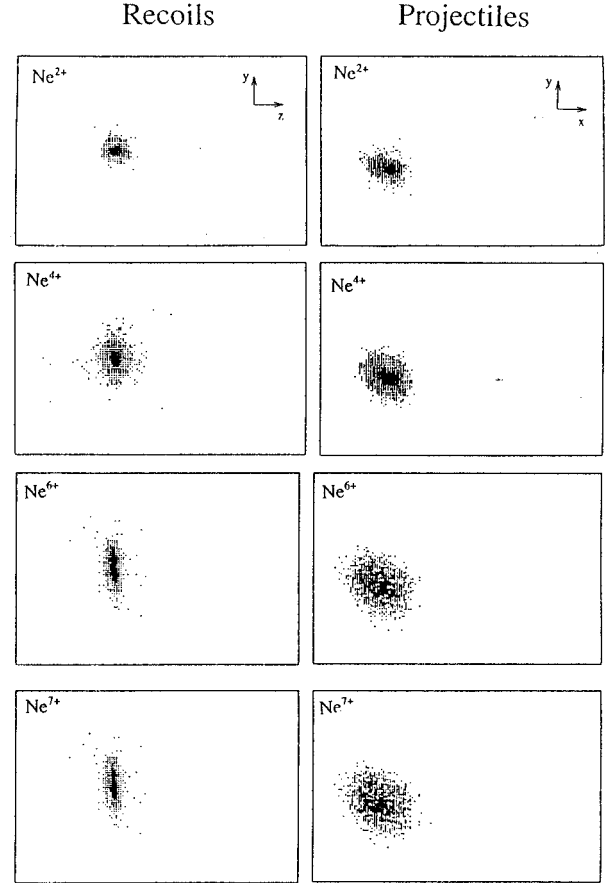


FIG. 3. Density plots of the momentum distributions for  $\text{F}^{9+}$  projectiles that have captured a single electron from Ne, for different final Ne charge states. The left-hand figures show the projections into the  $x$ - $y$  plane and are from the recoil momenta. The right-hand figures show projections into the  $X$ - $Y$  (transverse) plane taken from the projectile momenta; the transverse recoil momenta are nearly identical, as discussed in the text.

For the projectile ions, the experimental transverse momentum resolution is much worse than for the recoils and was dominated by the detector resolution and the beam optics. Using the  $\text{Ne}^{1+}$ ,  $\text{F}^{9+} \rightarrow \text{F}^{9+}$  channel as an experimental measurement of the projectile resolution function, we found that a two-dimensional Gaussian resolution function with  $\Delta P_x = \Delta P_y = 16.5$  a.u. gave a good fit to the data and this function was used in all analyses. For reference purposes we note that the initial momentum of a 1-MeV/amu  $\text{F}^{9+}$  projectile is  $2.21 \times 10^5$  a.u.

### III. RESULTS AND DISCUSSION

#### A. General appearance of the distributions

The raw data could be displayed in several two-dimensional slices, one of which is shown in Fig. 2, where a plot of the recoil charge state is shown plotted versus the  $x$  component of the projectile scattering angle for three final projectile charge states. The figure is characterized by several “islands” of events, each of which corresponds to a unique combination of recoil and projectile ion final charge states. Different final recoil charge states are resolved in this two-

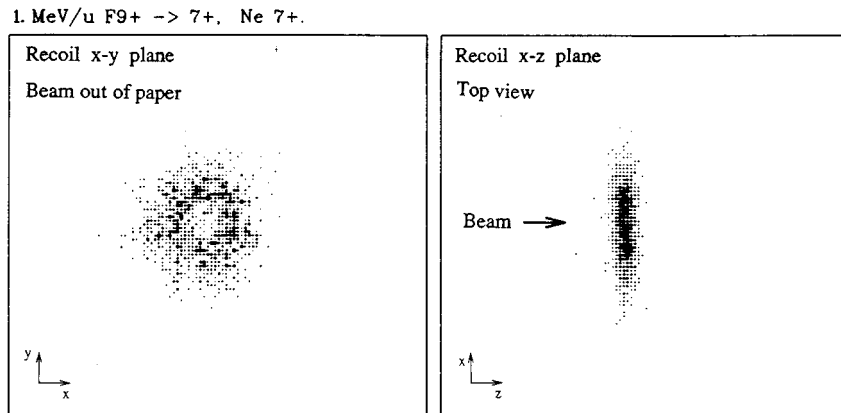


FIG. 4. Density plots of the recoil momentum distributions for  $F^{9+}$  projectiles that have captured two electrons and have left a  $Ne^{7+}$  recoil. The left-hand figure shows the projection transverse to the beam direction, and the right-hand figure shows a projection in a plane containing the beam direction.

dimensional figure, while they would not be resolved in a simple time-of-flight projection due to the “tilts” of the islands. The tilt is caused by the difference in flight times for recoils scattered towards and away from the recoil detector. The projectiles associated with these recoils are scattered in opposing directions in the  $x$  direction (time). The extensions to the right of the  $Ne^{3+}$  and  $Ne^{4+}$  islands are due to the  $^{22}Ne$  isotope. Events associated with a particular projectile and recoil final charge state were isolated by placing a software gate around the desired island and calculating, for each event, the recoil momentum vector and the transverse projectile momentum transfer vector. Roughly, the more electrons captured or ionized in the collision, the smaller the impact parameter. The evolution of the islands as one proceeds from soft (large impact parameter, low recoil, and projectile charge change) to hard (small impact parameter, large charge changing) collisions can be seen. The islands become more elongated and tilted for harder collisions, due to the larger scattering angles with respect to the beam direction.

The results of the momentum reconstruction process can be seen in Figs. 3 and 4. Figure 3 shows transverse and longitudinal momentum spectra for different recoil charge states for single electron capture (and retention) by the projectile. For this figure the transverse momenta were taken from the projectiles, although, as discussed below, the recoil transverse momentum spectra are nearly identical. The nature of the distributions evolves from nearly spherical for  $Ne^{2+}$  to very disklike for  $Ne^{7+}$ . The disk shape results from the fact that the transverse momentum transfer for the harder collisions greatly exceeds the longitudinal momentum transfer. Figure 4 shows similar spectra for harder collisions in which two electrons are captured by the projectile, displaying the disk structure but now with an absence of events in the center, indicating that very small impact parameters are required for double capture producing recoils as highly ionized as  $Ne^{7+}$ .

### B. Total ionization and capture cross sections

The relative ionization cross sections are proportional to the ratios of the number of ions in each collision channel, where the collision channel is defined as a specific postcol-

lision recoil-projectile charge state combination. In the present work all recoil charge states were collected simultaneously with two of the projectile charge states, so that for a given data run each partial ionization cross section was proportional to the ratio of the number of counts within the corresponding software gate. Although the simultaneous collection of the data eliminated most potential systematic errors, it was necessary to correct the data for double collisions using a spectrum-subtraction procedure similar to that described by Ali *et al.* [27]. To put the entire set of measurements on an absolute scale, we made a separate absolute measurement of the cross section for single capture, summed over all recoil charge states. For this experiment, the pusher was replaced with a gas cell of known length [28]. An absolute measurement of the pressure in the cell was made using a capacitance manometer. From the ratio of yields of  $F^{8+}$  and  $F^{9+}$  ions, we obtained a cross section

$$\sigma_{98} = (7.35 \pm 0.38) \times 10^{-17} \text{ cm}^2, \quad (5)$$

which was used to place all of our data on an absolute scale. The resulting cross sections are approximately 0.72 times the cross sections reported previously for this system by Gray *et al.* [29], a result consistent with the findings of Be *et al.* [30]. Total cross sections are shown in Fig. 5, which also shows the experimental values of Gray *et al.*, multiplied by 0.72, and theoretical nCTMC results. The error bars are based on experimental statistics, experimental background, uncertainty in the length of the gas cell due to aperture effects, and quality of charge state separation. Overall consistency with the normalized Gray *et al.* results is excellent, except for the highest recoil final charge states associated with double electron capture to the projectile, for which the cross sections are the most difficult to measure. The agreement of the nCTMC calculations with the experiment is good except for a slight shift in absolute scale. For the double capture collisions, the nCTMC calculation predicts a peak in the cross sections at  $Ne^{5+}$ , while the experimentally derived results show peaking at  $Ne^{7+}$ . The theoretical overestimation of the double capture cross sections is probably due to the neglect of autoionization of the doubly excited states produced in the capture reaction.

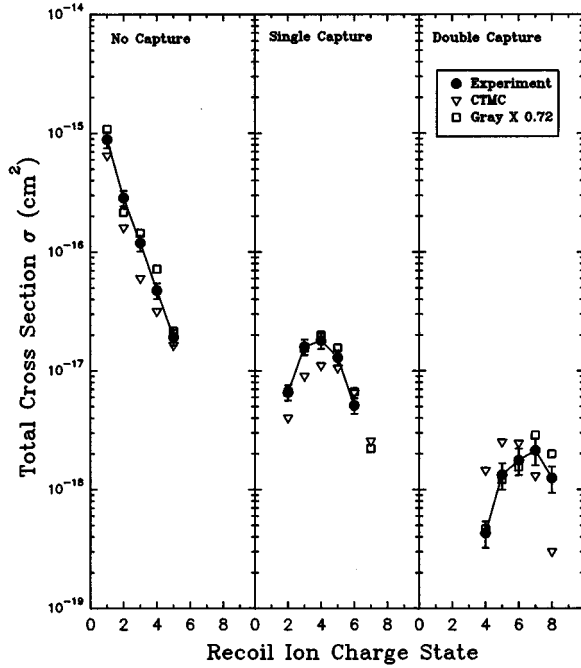


FIG. 5. Absolute cross sections for 1 MeV/u  $F^{9+}$  on Ne. The solid circles and open triangles are experimental and nCTMC points, respectively, from the present work. The open squares are from Gray *et al.* [29], reduced by 0.72.

### C. Transverse momentum distributions

#### 1. Comparison of recoil and projectile transverse momentum transfer

By comparing the projectile and recoil ion transverse momentum vectors, we can deduce the degree to which electrons remove net transverse momentum from the system. If

the contribution to the net transverse momentum of the electrons ionized to the continuum were negligible, we would expect that the transverse momentum of the recoil ions should be equal to and opposite that of the projectiles. We have investigated this point both through event-by-event comparisons of the momentum balance in individual collisions and through comparisons of the overall transverse momentum transfer distributions for projectiles and recoils. Figure 6 shows plots of the  $y$  components of recoil and projectile momentum transfer, for which we have the best overall resolution, for several representative collision systems. If recoil and projectile transverse momentum transfers are equal and opposite, the data should lie on a straight line with a slope of  $-1$ . This is seen clearly to be the case for the harder double capture collisions. That this is so for softer collisions is less obvious in this presentation of the data, because these plots are dominated by the experimental resolution.

A more comprehensive comparison of the final projectile and recoil transverse momentum distributions was performed by plotting the differential cross sections  $d\sigma/dp_{\perp}$  vs  $p_{\perp}$  for all available collision channels, shown in Fig. 7. Since the momentum resolution in the transverse direction for the recoils is much better than that for the projectiles, the comparison is made after folding the recoil distributions with a Gaussian resolution function with a FWHM of 16.5 a.u. (the resolution of the projectile distributions). This procedure is rigorously correct only if the recoil resolution is completely negligible, but is a good approximation here. The folding procedure has a strong effect on the distributions only for the lowest recoil charge states in the  $F^{9+} \rightarrow F^{9+}$  channel. The resulting distributions are seen to be nearly identical, confirming again that, within the resolution of the experiment, transverse momentum transfers of the two heavy partners balance.

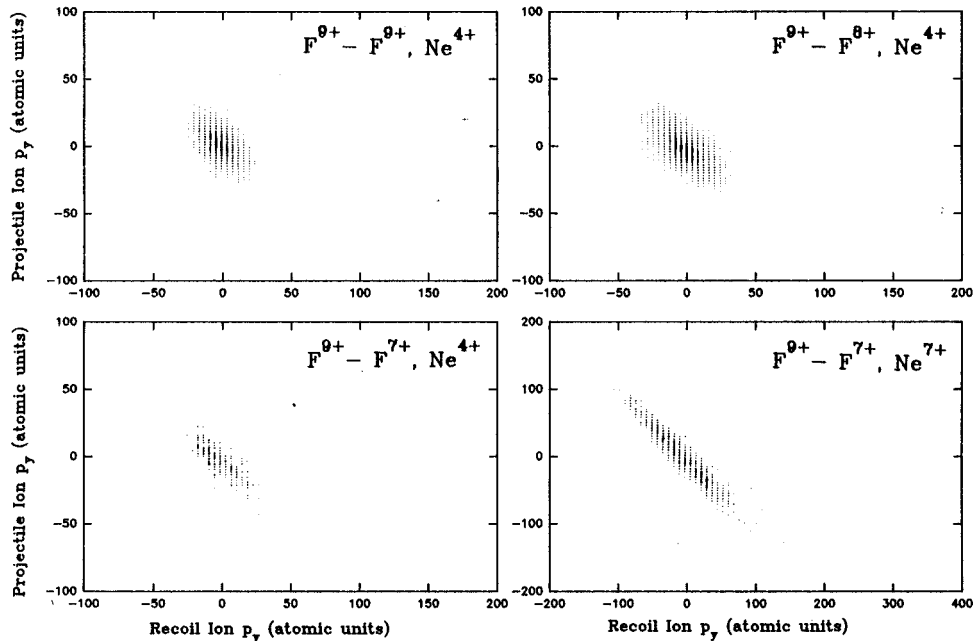


FIG. 6. Density plots of recoil  $y$  momentum versus projectile  $y$  momentum for four representative collision systems.

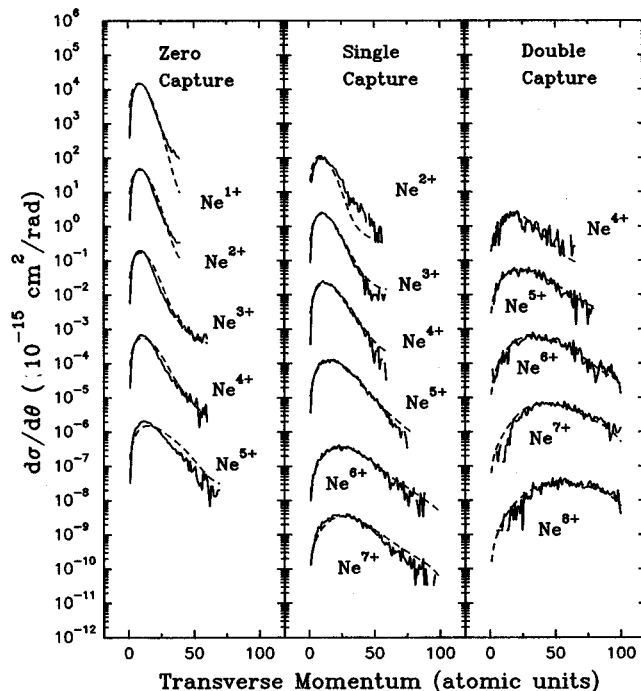


FIG. 7. Cross sections differential in scattering angle for the recoil and projectile ions. The uppermost curve for zero, single, and double capture is plotted on the absolute scale as labeled. For clarity of presentation, each successive curve below these has been shifted downward by an additional two decades. The experimental resolution function for the projectile ions has been folded into the recoil ion spectra.

## 2. Comparison with nCTMC calculations

Since the recoil and projectile transverse momentum distributions were found to be nearly identical, we chose to compare the recoil ion distributions, which have the better experimental resolution, with the nCTMC theoretical distributions. The comparison of the theoretical to the experimental was performed by folding the nCTMC results into the experimental recoil resolution function. The comparison is made in Fig. 8. Agreement between the shapes of the theoretical and experimental curves is good, although there is somewhat less agreement between nCTMC and experiment in absolute scales. Reasons for the small discrepancies are not at hand, although it might be noted that the nCTMC calculations do not include electron-electron interactions explicitly. The worst disagreement seems to occur for the hardest collisions, those involving double capture, for which  $K$  vacancy transfer might be playing an important role. A classical description of this process is probably not adequate. The agreement between experiment and theory for soft collisions seen here is much better than that seen by Lencinas *et al.* [16], who found experimental distributions that were substantially broader in transverse momentum transfer than the nCTMC results for a very similar collision system. The resolution of the present experiment is somewhat better than that possible with the cooled gas cell used by Lencinas *et al.*, and this may enable a better comparison between experiment and theory for small  $p_{\perp}$ .

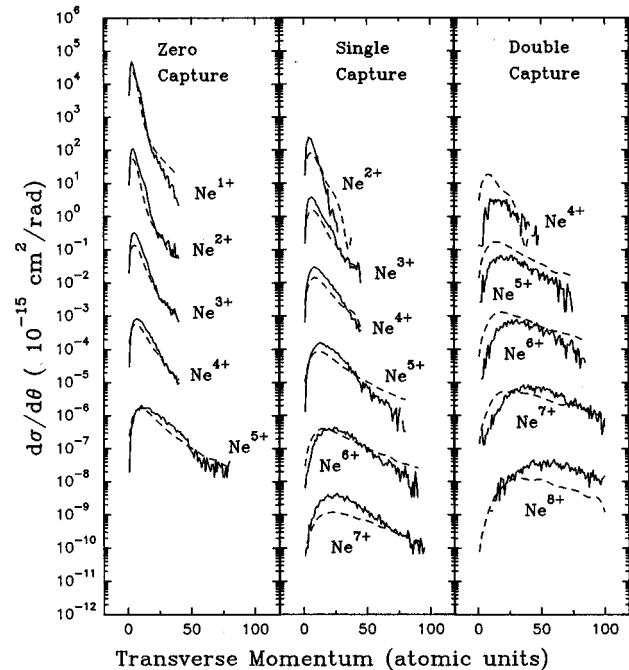


FIG. 8. Experimental cross sections differential in scattering angle for the recoil momenta (solid lines), compared to nCTMC calculations (dashed lines). The uppermost curve for zero, single, and double capture is plotted on the absolute scale as labeled. For clarity of presentation, each successive curve below these has been shifted downward by an additional two decades. The theoretical results have been folded into the experimental recoil resolution function.

## 3. Recoil energies

Historically, it has been more common to discuss transverse momentum distributions in terms of the energy distributions of the recoils, and we include a presentation of our data in these terms in order to facilitate comparisons and connections to earlier data. The energy distributions the recoil ions produced in such highly ionizing collisions have been a topic of discussion for many years, partly because of the information these distributions provide about the primary collision mechanism and partly because of the importance of the energy spreads in determining the brightness and energy resolution of secondary ion recoil sources [4]. Previous experiments have measured only the transverse energy of the recoils, but as we discuss further below and can be seen from Figs. 3 and 4, this energy generally is the dominant contribution. We present in Fig. 9 our transverse momentum distributions converted to recoil energy plots. We note that the technique of collimating the gas jet and using only one-half of the Maxwellian distribution results in an effective energy resolution below thermal, down to 5 meV in this case. The measured energies of the recoil ions range from 5 meV to 1 eV, where the lower number is due to the experimental resolution. The data are compared with the nCTMC calculations, folded into the experimental resolution functions. Rather good overall agreement is seen, as would be expected from the results of Fig. 8. This conclusion is similar to that reached by Ullrich *et al.* [10].

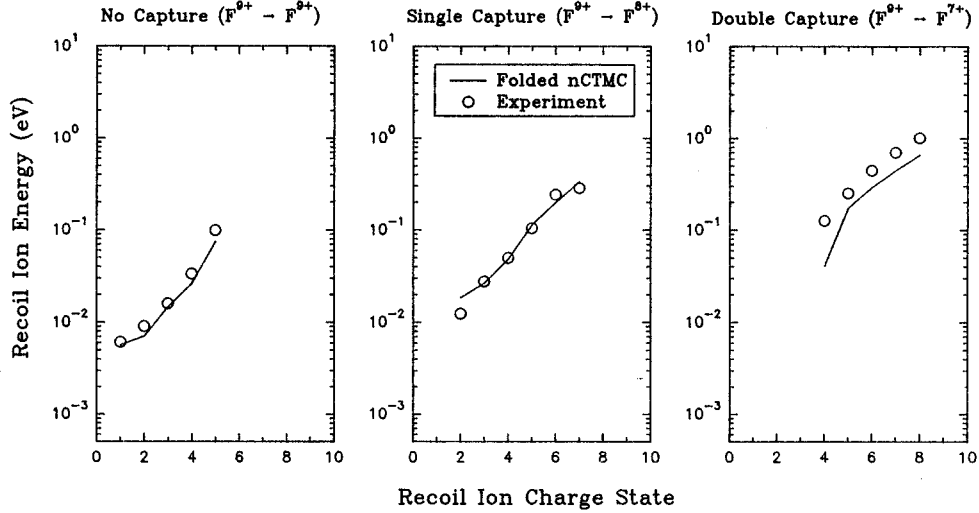


FIG. 9. Average (transverse) recoil ion energies for all collision channels (open circles), compared with the nCTMC predictions (solid lines). The latter are folded into the experimental resolution.

#### D. Recoil longitudinal momentum distributions

The centroids of the longitudinal momentum distributions from this work have been reported previously in Ref. [31]. For completeness, we include here the full  $p_z$  distributions, and offer an additional model interpretation of earlier data that has not been previously presented. A set of the  $z$  momentum spectra for the ionization, single capture, and double capture collision channels is shown in Fig. 10. The widths of the peaks are dominated in nearly all cases by the experimental resolution in the  $p_z$  direction of 10 a.u. The vertical lines indicate where  $p_z=0$  and the beam direction runs from left to right. Backward scattering can clearly be seen in this figure for collisions in which electrons are captured by the projectile. The centroids in  $p_z$  deduced from these data are shown in Fig. 11 and are seen to never exceed 8 a.u., much smaller than the transverse momentum transfer for all collision channels. The application of energy and momentum conservation for a two-body collision for small scattering angles leads to the result [32] that

$$p_z = -Q/v - n\mu v/2 - p_{ze}, \quad (6)$$

where  $Q$  is the increase of electronic binding energy in the collision (positive for exoergic collisions),  $n$  is the number of electrons transferred from the target to the projectile,  $\mu$  is the electron mass, and  $p_{ze}$  is the net longitudinal momentum carried by all final continuum electrons, measured in the target rest frame. Although the collisions studied here are far from two body in nature, the above expression nevertheless remains useful in discussing certain aspects of our data. In particular, the effect of the  $n\mu v/2$  term is seen clearly when one compares the  $p_z$  centroids for cases in which no capture occurs with those for which one to three electrons are captured. The nCTMC calculations also shown in Fig. 11 are in agreement with the data on this point.

Schuch *et al.* [25] and Schöne *et al.* [26] have previously shown that the projectile in similar collisions ( $C^{6+}$  on Ne at 10 MeV/u) can be expected to lose up to 1.5 keV in a collision that creates a  $Ne^{6+}$  recoil and captures no elec-

trons. Such an energy loss by the projectile implies that the projectile would lose 8.75 a.u. of  $P_z$  and thus either the recoil ion or the continuum electrons or both must travel forward with this momentum after the collision. Our data for  $F^{9+}$  to  $F^{9+}$  show clearly that this momentum is nearly entirely carried by the continuum electrons, not by the recoil ion. This result is qualitatively in agreement with the recent results of Moshhammer *et al.* for  $Ni^{24+}$  on He [33] and of Dörner *et al.* [12] for  $p$  on He and shows that direct ionization events generally impart little longitudinal momentum to the recoil. Indeed, in both of the He target cases, the He recoils were found to recoil slightly backward rather than forward. On the scale of the  $Q/v$  of the present experiments, the recoil is left nearly at rest in an ionization dominated collision.

The only substantive disagreement between nCTMC calculations and the data lies in the recoil charge state dependence of the  $p_z$  centroid for a fixed number of electrons transferred. The data show that the higher the recoil charge state, the less backward the recoil is thrown, while the nCTMC calculation shows the opposite trend. No complete explanation of this disagreement is at hand, but we offer some observations on this point. First, the nCTMC calculations do not include the rearrangement effects due to Auger decays of either projectile or target ion. Especially for the close collisions it is to be expected that  $K$  to  $K$  vacancy transfer [34] will play an important role, leaving  $K$  vacancies often in the target. The Auger rearrangements following such a process will increase the charge of the measured recoil relative to that predicted by the nCTMC calculation presented in Fig. 11 and will thus tend to wash out the increasingly backward kicks predicted by the calculation. Quantitative evaluation of the size of this effect is difficult. Second, we note that the increase with recoil charge state of  $p_z$  follows closely the increase in  $Q/v$  that would result if the electrons captured were the “last ones” (i.e., most tightly bound on the Ne ion). For example, the increase in  $Q/v$  for single electron capture in going from  $Ne^{1+}$  to  $Ne^{2+}$  would be the difference between the ionization potential of  $Ne^{1+}$

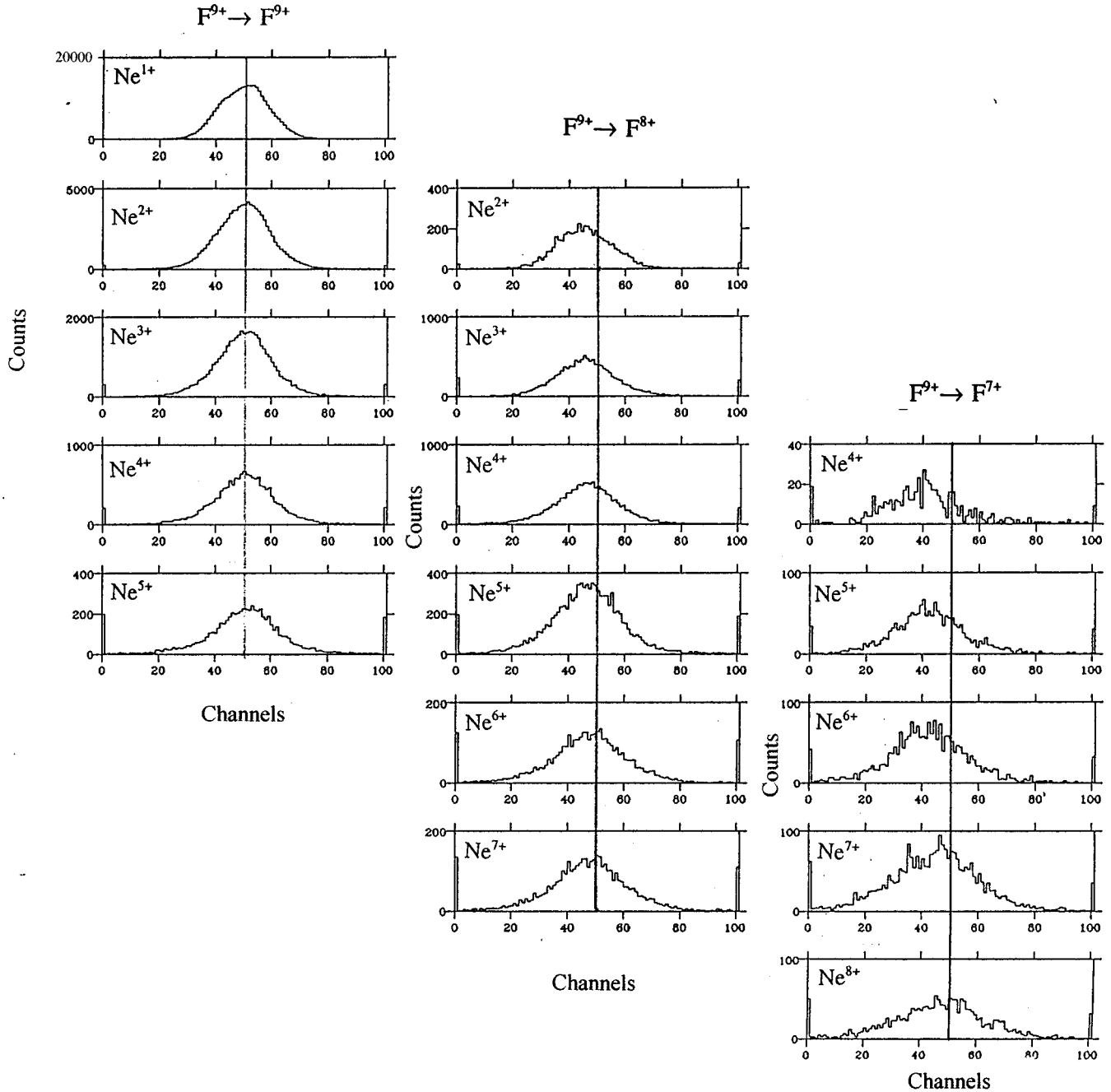


FIG. 10. Recoil  $p_z$  (longitudinal) distributions for zero-, one-, and two-electron capture. The vertical lines at channel 50 indicate the positions of  $p_z=0$  and the calibration is 0.5 a.u. per channel.

(1.5 a.u.) and that of neutral neon (0.79 a.u.), divided by the beam velocity of 6.35 a.u. This calculation presumes that the state(s) into which the electron is captured does not change. In Fig. 11 we have plotted this trend of  $Q/v$  versus recoil charge state for each capture channel, arbitrarily setting this term equal to zero for the pure capture recoil charge state for each final projectile charge state. Roughly, this amounts to assuming that the electrons lost to the continuum do not affect the recoil momentum directly at all, a conjecture sup-

ported by the absence of any recoil  $P_z$  for the  $F^{9+} \rightarrow F^{9+}$  case, and that the binding energy of the final capture state does not vary with recoil charge state. The trend of  $Q/v$  from this model is seen to follow the data rather closely, suggesting that the reason for the decreasingly backward-thrown recoils for higher recoil charge state is due to the requirement that the projectile must dig increasingly deeper on the target in order to obtain the captured electrons. This interpretation does not explain the discrepancy with the nCTMC results,

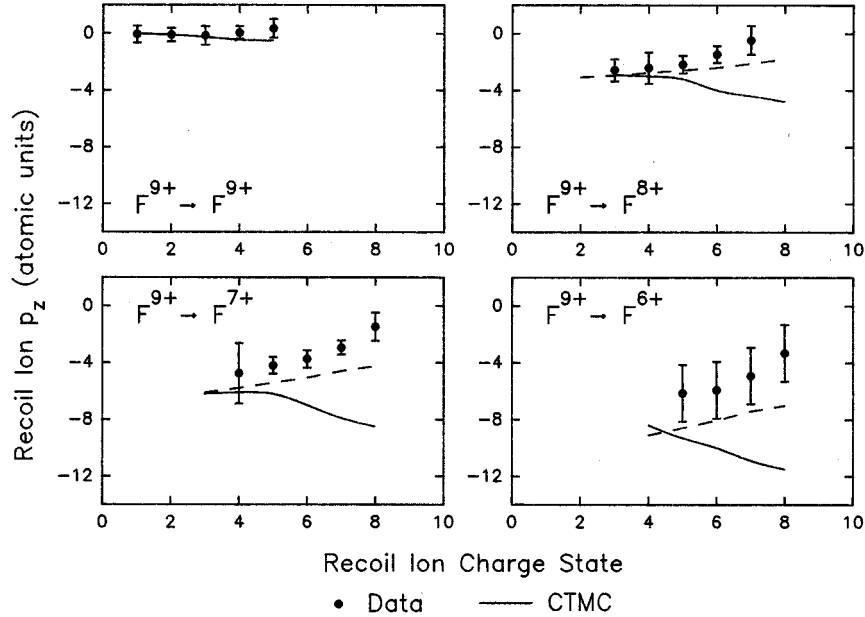


FIG. 11. Mean values of  $p_z$  as a function of recoil charge state for all collision systems. The filled circles are the experimental data and the solid lines the nCTMC results. The dashed lines show the variation with recoil charge state which would be expected if only the changing binding energy of the “last” captured electrons were taken into account (see the text).

however, since this effect is included in the dynamics of the nCTMC calculation.

#### IV. CONCLUSIONS AND SUMMARY

For the collision system  $F^{9+}$  on Ne, we have measured, for each final channel identified by projectile and recoil charge state, the full momentum vector of the recoil ion and the transverse momentum vector of the recoil. The recoil momentum distributions evolve from quasispherical (lying within the experimental resolution) for soft collisions characterized by small recoil charge to disk-shaped for hard collisions producing high recoil charge states. The recoil transverse momentum transfers are found to substantially exceed the longitudinal momentum transfers in general. The transverse momentum imparted to the projectile is found to be nearly balanced, within an experimental resolution of a few a.u., by an opposite transverse momentum given to the recoil ion. Thus the net mean momentum carried away by up to six continuum electrons is seen to be much smaller than that imparted to the heavy-ion cores in such collisions. The absence of any essential role played by transverse momentum imparted to the continuum electrons is in disagreement with the results of Gonzalez *et al.* [35]. It is in contrast to the established result for the much lighter system of  $p + \text{He}$ , studied by Doerner *et al.*, for which there is a substantial mismatch of transverse momenta between projectile and recoil. We note that the momentum scale subjected to experimental scrutiny here is limited by the experimental resolution (7 a.u.) and that imbalances on a scale smaller than this cannot be seen in the present data. The projectile energy loss results for  $C^{6+}$  on Ne indicate mean continuum electron

energies of order 200 eV, or about 4 a.u. of momentum per electron. That the mean vector momentum of several electrons ejected with such a momentum should not exceed our experimental resolution is perhaps not surprising, but also not *a priori* certain. The transverse momentum distributions are generally in good agreement with the nCTMC predictions, except for the very highest recoil charge states. The longitudinal recoil momentum is found to be small, below 2 a.u. for the direct ionization  $F^{9+} \rightarrow F^{9+}$  channel, for all recoil charge states. When coupled with the knowledge that the projectile loses considerable energy in the collision, this result implies that the continuum electrons carry away most of the longitudinal momentum lost by the projectile in the collision. For the capture channels, the backward shift due to the  $n\mu\nu/2$  term in Eq. (3) is clearly seen for low charge state recoils, and good agreement with the nCTMC calculation is seen. The higher charged recoils are thrown more forward than is predicted by the nCTMC calculation. Some speculation is offered that this may be due to the necessity of removing increasingly tightly bound electrons from the target in order to attain a highly charged recoil in coincidence with capture. However, the discrepancy with the nCTMC calculation remains.

#### ACKNOWLEDGMENTS

We thank R. Dörner, J. Ullrich, H. Schmidt-Böcking, S. Lencinas, and S. Hagmann for stimulating discussions. This work was supported by the Division of Chemical Sciences, Office of Basic Energy Sciences, Office of Energy Research, U.S. Department of Energy.

- [1] Fifteenth International Conference on Atomic Collisions in Solids, edited by M. Zinke-Allmang, W.N. Lennard, and G.K. Massourni [Nucl. Instrum. Methods Phys. Res. Sect. B **90**, 1 (1994)]; Tenth International Conference on Ion Implantation Technology, edited by S. Coffa, G. Feila, F. Priolo, and E. Rumini [Nucl. Instrum. Methods **96**, 1 (1995)].
- [2] GSI Scientific Report, March 1994, pp. 203–222 (unpublished).
- [3] Fifth International Workshop on Atomic Physics for Ion Driven Fusion, edited by J. Meyer-ter-Vehn [Laser Part. Beams **8**, 523 (1990)].
- [4] C.L. Cocke and R.E. Olson, Phys. Rep. **205**, 153 (1991).
- [5] J.C. Levin, R.T. Short, C.-S. O, H. Cederquist, S.B. Elston, J.P. Gibbons, and I.A. Sellin, Phys. Rev. A **36**, 1649 (1987).
- [6] J.C. Levin, R.T. Short, C. Biedermann, H. Cederquist, S.B. Elston, C.-S. O, and I.A. Sellin, Phys. Rev. A **49**, 228 (1994).
- [7] J. Ullrich *et al.*, Nucl. Instrum Methods Phys. Res. Sect. A **268**, 216 (1988).
- [8] R. Dörner *et al.*, in *Invited Papers of the XVIIth International Conference on the Physics of Electronic and Atomic Collisions*, edited by W.R. MacGillivray *et al.* (Hilger, London, 1992), Vol. 351.
- [9] J. Ullrich *et al.*, Comments At. Mol. Phys. **30**, 285 (1994).
- [10] J. Ullrich *et al.*, J. Phys. B **22**, 627 (1991).
- [11] G.P. Grandin, D. Hennecart, X. Husson, D. Lecler, I. Lesteven-Baisse, and D. Lisfi, Europhys. Lett. **6**, 683 (1988).
- [12] R. Dörner, J. Ullrich, R.E. Olson, O. Jagutzki, and H. Schmidt-Böcking, Phys. Rev. A **47**, 3845 (1993).
- [13] J. Ullrich, M. Horbatsch, V. Dangendorf, S. Kelbch, and H. Schmidt-Böcking, J. Phys. B **21**, 611 (1988).
- [14] J. Ullrich, R.E. Olson, R. Dörner, V. Dangendorf, S. Kelbch, H. Berg, and H. Schmidt-Böcking, J. Phys. B **22**, 627 (1989).
- [15] V. Mergel *et al.*, Phys. Rev. Lett. **74**, 2200 (1995).
- [16] S. Lencinas *et al.*, J. Phys. B **26**, 287 (1993).
- [17] R.E. Olson, J. Ullrich, and H. Schmidt-Böcking, Phys. Rev. A **39**, 5572 (1989).
- [18] M. Horbatsch, J. Phys. B **25**, 3797 (1992).
- [19] R. Ali *et al.*, Phys. Rev. Lett. **69**, 2491 (1992).
- [20] W. Wu *et al.*, Phys. Rev. A **51**, 3718 (1995).
- [21] W. Wu *et al.*, Phys. Rev. A **50**, 502 (1994).
- [22] M.L.A. Raphaelian *et al.*, Phys. Rev. A **51**, 1304 (1995).
- [23] W. Wu, Phys. Rev. Lett. **72**, 3170 (1994).
- [24] R. Dörner *et al.*, Phys. Rev. Lett. **72**, 3166 (1994).
- [25] R. Schuch, H. Schöne, P.D. Miller, H.F. Krause, P.F. Dittner, S. Datz, and R.E. Olson, Phys. Rev. Lett. **60**, 925 (1988).
- [26] H. Schöne *et al.*, Phys. Rev. A **51**, 324 (1995).
- [27] R. Ali *et al.*, Phys. Rev. A **49**, 3586 (1994).
- [28] J. Sanders, Ph.D. dissertation, Kansas State University, 1992 (unpublished).
- [29] T.J. Gray, C.L. Cocke, and E. Justiniano, Phys. Rev. A **22**, 849 (1980).
- [30] S.H. Be *et al.*, J. Phys. B **19**, 1771 (1986).
- [31] V. Frohne, S. Cheng, R. Ali, M. Raphaelian, C.L. Cocke, and R.E. Olson, Phys. Rev. Lett. **71**, 696 (1993).
- [32] M.R.C. MacDowell and J.P. Coleman, *Introduction to the Theory of Ion-Atom Collisions* (North-Holland, Amsterdam, 1970), p. 375.
- [33] R. Moshhammer *et al.*, Phys. Rev. Lett. **73**, 3371 (1994).
- [34] A. Skutlartz and S. Hagmann, Phys. Rev. A **28**, 3268 (1983).
- [35] A.D. Gonzalez, S. Hagmann, T.B. Quinteros, B. Krassig, R. Koch, A. Skutlartz, and H. Schmidt-Böcking, J. Phys. B **23**, L303 (1990).